Synthesis and Characterization of ZnO and Fe₃O₄ Nanocrystals from Oleat-based Organometallic Compounds

PoiSim Khiew[1, *], WeeSiong Chiu[2], ThianKhoonTan[1], Shahidan Radiman[3], Roslan Abd-Shukor[3],Muhammad Azmi Abd-Hamid[3], ChinHua Chia[3]

Abstract—Magnetic and semiconductor nanomaterials exhibit novel magnetic and optical properties owing to their unique size and shape-dependent effects. With shrinking the size down to nanoscale region, various anomalous properties that normally not present in bulk start to dominate. Ability in harnessing of these anomalous properties for the design of various advance electronic devices is strictly dependent on synthetic strategies. Hence, current research has focused on developing a rational synthetic control to produce high quality nanocrystals by using organometallic approach to tune both size and shape of the nanomaterials. In order to elucidate the growth mechanism, transmission electron microscopy was employed as a powerful tool in performing real time-resolved morphologies and structural characterization of magnetic (Fe₃O₄) and semiconductor (ZnO) nanocrystals. The current synthetic approach is found able to produce nanostructures with well-defined shapes. We have found that oleic acid is an effective capping ligand in preparing oxide-based nanostructures without any agglomerations, even at high temperature. The oleate-based precursors and capping ligands are fatty acid compounds, which are respectively originated from natural palm oil with low toxicity. In comparison with other synthetic approaches in producing nanostructures, current synthetic method offers an effective route to produce oxide-based nanomaterials with well-defined shapes and good monodispersity. The nanocysrals are well-separated with each other without any stacking effect. In addition, the as-synthesized nanopellets are stable in terms of chemically and physically if compared to those nanomaterials that are previous reported. Further development and extension of current synthetic strategy are being pursued to combine both of these materials into nanocomposite form that will be used as "smart magnetic nanophotocatalyst" for industry waste water treatment.

Keywords—Metal oxide nanomaterials, Nanophotocatalyst, Organometallic synthesis, Morphology Control

I. INTRODUCTION

THE design of electronic devices by using nanomaterials is massively dependent on the congruent electronic properties of the particular nanomaterials. However, the electronic property is highly influenced by the structural dimension of the nanomaterials. For instances in 1-D semiconductor nanostructures, the quasi-continuous density of states exhibits singularities near the band edges followed by exponentially decay while that of 2-dimensional semiconductor nanostructures is partially discrete [4, 5]. Substantial variation in electrical and optical properties in accordance to the dimensional changes can be observed when the particular electronic energy gap exceeds the thermal energy. Some examples of remarkable 2-dimensional quantizes effects are integer and fractional quantum hall effects [6-9]. Therefore, a routine method in preparing 2-dimensional semiconductor nanostructures should be developed to unravel the shape-guiding effects. Recently, oxide based semiconductor nanomaterials also become subject of study due to their thermal- and photo-stability [10]. Among these nanomaterials, ZnO is the well-known candidate due to its relatively wide band gap energy (3.37 eV). This property enables the ultraviolet lasing effects to be observed even at room temperature [11-13]. In addition, the exciton binding energy of ZnO (60 meV) is much larger than thermal energy at room temperature (26 meV) if compared to other semiconductor materials such as ZnSe (22 meV) [14] or GaN (25 meV) [15]. On the other hand, magnetic iron oxide (Fe₃O₄) nanocrystals have long been of scientific and technological interest. The cubic spinel structured MFe₂O₄ represents a well-known and important class of iron oxide materials where oxygen forms an fcc close packing, and M^{2+} and Fe^{3+} occupy either tetrahedral or octahedral interstitial sites. By adjusting the chemical identity of M^{2+}, the magnetic configurations of MFe₂O₄ can be molecularly engineered to provide a wide range of magnetic properties. Although there has been a great deal of recent works on oxide materials preparation, in comparison, the research works are still considerably lagging behind on the state of the art of chalcogenide-based and noble metal nanostructures. This phenomenon could be attributed to the poor synthesis method and less suitably applicable capping ligands (only used in solution-phase synthesis) for high temperature synthesis process while this high temperature synthesis process (in gas-phase synthesis) is favored for oxidation reaction to occur. Furthermore, the apparatus setup at such high temperature reactor for gas-phase synthesis of oxide-based nanostructures is very complicated. Consequently, all the obstacles mentioned above in both gas and solution-phase syntheses have limited the studies of monodisperse nanostructures. Hereby, we report the size and shape control synthesis of magnetic (Fe₃O₄) and semiconductor (ZnO) nanocrystals in solution-phase using thermal sustainable organic compound (oleic acid) as capping ligands. We have found that oleic acid is an effective capping ligand in preparing oxide-based nanostructures without any

[1]Faculty of Engineering, University of Nottingham Malaysia Campus, Jalan Broga, 43500 Semenyih, Selangor, Malaysia. (phone: + 603-89248179; fax: +603-89248179; email:PoiSim.Khiew@nottingham.edu.my)
[2]Low Dimensional Materials Research Center, Department of Physics, Faculty of Science, University Malaya, 50603 Kuala Lumpur, Malaysia
[3]School of Applied Physics, Faculty Science and Technology, University Kebangsaan Malaysia, 43600 Bangi, Selangor, Malaysia

agglomerations even at elevated processing temperature. The oleate-based precursors and capping ligands that have been used in the current study are fatty acid compounds, which are originated from natural palm oil with low toxicity. Hence the current synthetic approach offers an inexpensive, safe and facile synthesis route to produce oxide-based nanomaterials with high yield.

II. EXPERIMENTAL METHODOLOGY

A. Synthesis of Fe_3O_4 Nanocrystals

The pyrolysis reaction was carried out in a 250 ml four neck flask equipped with a condenser and a heating mantle (Fig. 1). In a typical synthesis, 3 milimol iron oleate precursor and 1.5 milimol oleic acid were dissolved in 40 ml hexadecane. The mixture was heat at 287 ^{o}C and refluxed for 60 minutes under inert atmosphere. The desired size of the nanocrystals was obtained by manipulating the refluxing time. The reaction was terminated by removing the flask from the mantle and cooled to room temperature by the flowing of Ar gas. Excessive of acetone was added to precipitate nanocrystals follow by dispersing in hexane. The processes of precipitating and dispersing were repeated for three times to purify the nanocrystals. Finally, the nanocrystals were dried in vacuum desiccators overnight.
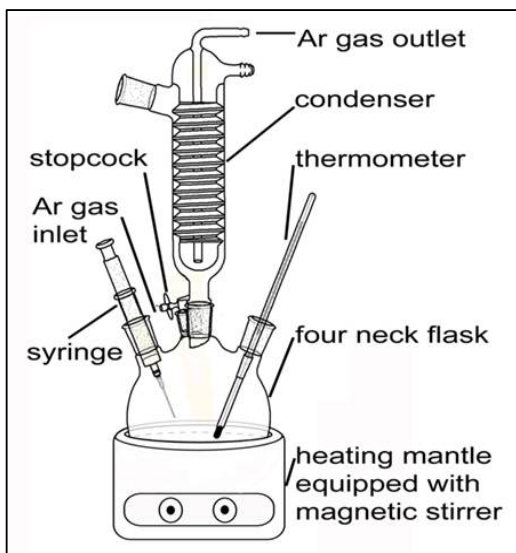

Fig. 1 Apparatus setup for the synthesis oxide-based nanocrystals

B. Synthesis of 2-dimensional ZnO Nanopellets

The reaction was carried out under aerated argon atmosphere in a 250 ml four-neck flask equipped with a condenser, as shown in Fig. 1 as well. In a typical synthesis, 10 milimol $Zn(C_{18}H_{33}O_2)_2$ and 5 milimol oleic acid ($C_{18}H_{34}O_2$, Sigma Aldrich, 99%) were dissolved in 115 ml n-octadecene after being continuously heated at 85 ^{o}C for 1 hour. Afterwards, evacuation for 30 minutes was done repeatedly with mechanical pump to eliminate the oxygen and residual water. Then, the temperature of the mixture was ramped to 317 ^{o}C

with a constant heating rate and refluxed for various durations of time (60 minutes, 90 minutes and 120 minutes). The presence of grey precipitation indicates the formation of ZnO nanopellets. In order to separate the precipitates, excessive amount acetone was added and the precipitate was redispersed in hexane. The processes of precipitating and dispersing were repeated for three times to remove the impurities. Finally, the precipitates were dried in a vacuum desiccator overnight.

C. Instrumental Characterization

The morphology of two-dimensional nanocrystals was characterized by transmission electron microscope (TEM) (Philips CM12 with operation voltage 100 kV). The crystal structures was identify by X-ray diffraction (XRD using Bruker AXS-D8 Advance Diffractometer (scanning rate 0.01^{o}/s, Cu-Kα radiation and wavelength, λ = 0.154 nm). The element analysis was performed by energy dispersion X-ray analysis (EDXA) by using Leo 1450 VPSEM instrument operated with acceleration voltage 15 keV.

III. RESULTS AND DISCUSSIONS

A. Transmission Electron Micrograph (TEM)

Many research works have indicated that oleic acid can be used as a versatile ligand/solvent for the synthesis of novel nanocrystals because of the tunable reactivity and relatively high boiling point. A control ramp of temperature promotes the dissolution of the iron oleate precursor. At critical threshold, supersaturation was achieved. The supersaturation was relieved by a fast but short outburst of nucleation to form nucleus. The subsequent growth occurred by depositing the constituent elements onto the seeds of Fe_3O_4. In order to obtain nanocrystals with narrow size distribution, secondary nucleation must be inhibited.
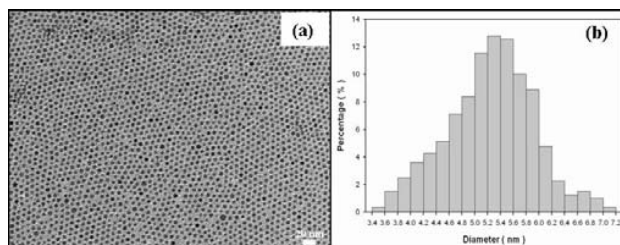

Fig. 2 (a) Low resolution of TEM micrograph of Fe_3O_4 nanocrystals prepared with heating duration 60 min (which self-assembled into monolayer) (b) Particles size distribution of the as prepared Fe_3O_4 nanocrystals

The decomposition rate of the precursor was adjusted until it is equal or less than the rate at which the constituent elements are deposited to the nucleus seed. Further growth is limited by diffusion of the constituent elements to the nuclei surface, which is a slow and long process. This is agrees with LaMer mechanism that predicts the needed key separation of nucleation and growth in time, which is required for the formation of monodisperse size distribution. Further annealing by refluxing is necessary to trigger atomic diffusion within nanocrystals to allow atoms to adopt correct positions to

develop into crystal lattices. TEM image for sample prepared by heating duration 60 min is shown in Fig. 2(a). These solids resemble the random packing of hard spheres with soft shells (ligands) filling the interstices.The histogram (Fig. 2(b)) shows the size distribution of nanocrystals with mean size and standard deviation of 5.2 nm and 0.8 nm (15.3% of mean value), respectively. By manipulating the refluxing period, the desired size of the nanocrystals can be obtained. It is found that the sizes of nanocrystals increased with reaction time. According to Reiss model, control surface diffusion-limited growth is a key factor in growing monodisperse particles. At the same time, the distribution of nanocrystals is broadened when the heating duration is increased. This is due to the Ostwald ripening process.By controlling the solvent evaporation rate, the nanocrystals can be self-assembled in monolayer (Fig. 2(a)) and triangle "island" in an ordered hexagonal closed-pack superlattices (Fig. 3). In order to obtain monolayer (Fig. 2(a)), the ratio of the volume of hexane to the volume of ethanol is adjusted to 2:1. Such composition allows the nanocrystals to have sufficient time to diffuse into the empty space on the surface of the copper grid. From the TEM micrograph, the darker spots originated from nanocrystals due to the backscattering of electron beams while the white spots that surrounded the nanocrystals are attributed to the oleic acid that passivated the surface of the nanocrystals. This space allowed the penetration of electron beam. Oleic acids have played a very important role by providing a stearic barrier to avoid the nanocrystals from aggregating. Some of the nanocrystals look "darker" due to the enhancement of electron diffraction contrast caused by different orientations of lattice fragments with respect to the electron beam.In order to increase the solvent evaporation rate, the volume ratio of hexane to ethanol is adjusted to 8:2. The self-assembly of nanocrystals exist in a bi-layer form where the second layer is positioned in the interstices of the previous layer (Fig. 3.). Therefore, by increasing of the evaporation rate, it will lead to a condition which the nanocrystals do have not enough time to fully diffused and deposited on the surface of the copper grid directly. Hence, major local defects will form since not the entire surface of the copper grid is fully covered by nanocrystals [8]. The locations that individual nanocrystals arrange themselves provide the greatest number of nearest neighbors to maximize attractive forces within the hexagonal close-packed structures. These attractive forces arise from Van der Waal's and dipolar magnetic interaction among the nanocrystals that provide the most stable state [9].
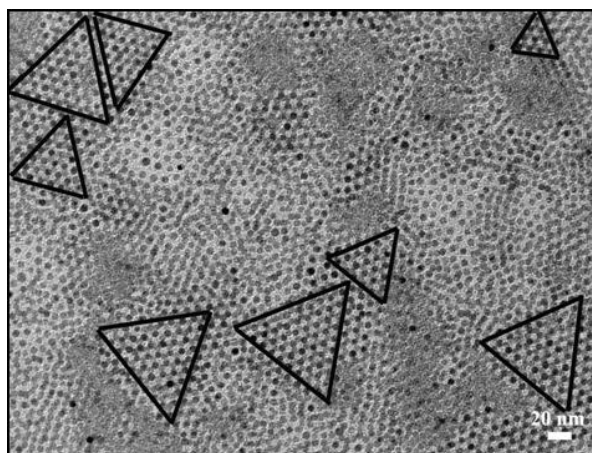

Fig. 3 Triangle "island" of Fe_3O_4 nanocrystals, ordered in hexagonal closed-pack superlattices

TEM micrograph of ZnO crystals annealed at 317 °C for 60 minutes is shown in Fig. 4. The average edge length is between 30 nm – 120 nm. Typically, the crystals exist in two-dimensional pellets with irregular shapes. The surfaces of the nanopellets are rough and stacked with many primary grains, which could be attributed to incomplete atomic diffusion. The densities of small primary grains for some of the nanopellets are high along their edges if compared their centers, as can be seen in TEM micrograph.
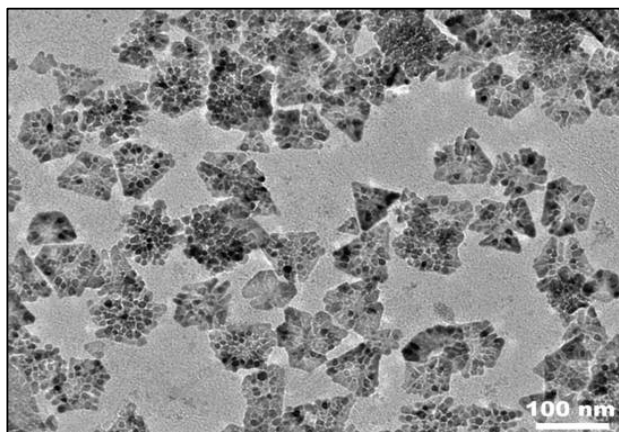

Fig. 4. TEM micrograph (magnification 35000 x) of ZnO nanopellets annealed at 317 °C for 60 minutes

In comparison with report by Yoshida et al. who utilized the water-soluble tetrasulfonated metallophthalocyanines (TSPsMs where M = Zn^{2+}, Al^{3+}, Si^{4+}) as capping ligands to synthesis two-dimensional ZnO nanopellets [34], the as-prepared ZnO nanopellets were found to have thickness around 1 μm. This could be attributed to the "bridging effect" of TSPsMs that allows the further growth of new ZnO disk planes on it and this "bridging effect" subsequently causes the stacking disks structure to be observed. The as-synthesized ZnO nanopellets in this study by using oleic acid as capping

ligands on the other hand is found manage to tune the nanopellets with thickness less than or equals to 10 nm which is much thinner. The growth of the primary nuclei along c-axis is inhibited due to the adsorption of oleic acid to the corresponding surface of the growing crystal, where no "bridging effect" has been observed as oleic acid provides greater stearic hindrances to inhibit the deposition of new plane on the initial disk plane. There are many research reports have indicated that oleic acid, which functions as coordinating agent can selectively bind on the specific crystal face(s) and regulate the growth and orientation of the surfaces kinetically [37-40]. Detailed studies by Wang et al. revealed that ZnO are highly polarized materials with chemically active Zn^{2+} terminated ZnO (0001) polar surface while the O^{2-} terminated (000$\bar{1}$) polar surface is inert [41]. Therefore, the negative charge alkyl chain $((C_{18}H_{33}O_2)^-)$ of oleic acid was found strongly bound on the highly polarized Zn^{2+} surface. As a result, further crystal growths occurred via continuous deposition of constituent element Zn^{2+} along a-axis and b-axis rather than c-axis. Hence, the primary ZnO crystals exist in two-dimensional thin pellet form with higher grain density along the edge of the crystal rather than that of the center (Fig. 4).Further increasing the duration of annealing to 90 minutes caused nanopellets to exist in well-defined shapes with flat edges (Fig. 5). This sample has shown "shape distribution" with the presence of both triangular and hexagonal nanopellets. The edge length of this sample falls within the range of 40 nm – 125 nm, which is larger compare to the sample that were being annealed for 60 minutes. The densities of the primary grains on the edges of the nanopellets become lower and this could be attributed to the complete atomic diffusion process.
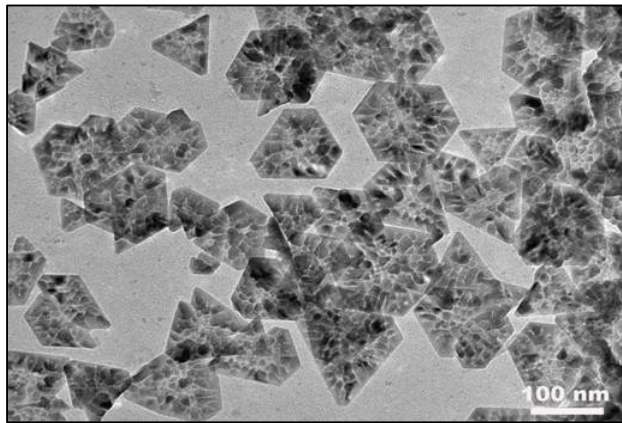

Fig. 5 TEM micrograph (magnification 35000 x) of ZnO nanopellets annealed at 317 °C for 90 minutes

Prolong annealing duration have triggered the tendency in minimizing the overall surface energy by promoting atomic diffusion, which subsequently decreased the surface area of the primary grains [42-44]. The primary grains along the edges of the individual crystal were highly unstable due to the low atomic packing density. The morphologies obtained from the 90 minutes sample were believed to provide higher energy areas that promoted grain boundary formation.

After the sample is exposed to a finite cumulative period of annealing for 90 minutes, the thermal energy absorbed had sufficiently triggered the surface atomic migration, followed by reorganization of the atom into the correct positions where the crystal lattices were formed. Subsequent thermal annealing caused the coalescence of small grains. These aggregates were separated by the grain boundaries on the surface as the result of thermally activated mass transport process. With prolonged annealing, the coalescence among the grain boundaries induced the emergence of the strong texturing surface. The sintering effect of the grains can also be observed from Fig. 5(a), which has shown rather smoother surfaces along the grain boundaries. This phenomenon is well-correlated with molecular dynamics simulations reported by Zhu et al. [45]. The effects of annealing duration on the shape of nanopellets was investigated by performing high magnification TEM imaging in order to observe the surface morphology on the selected ZnO nanopellets. As can be seen in Fig. 6 (a), the ZnO nanopellets are triangle in shapes with flat equilateral edge. Apparently, the truncated edge is also observed along each corner of the triangular nanopellet (highlighted in Fig. 6 (a)). Fig. 6 (b) indicates one of the "diamond shape" nanopellets with improved truncated edges.
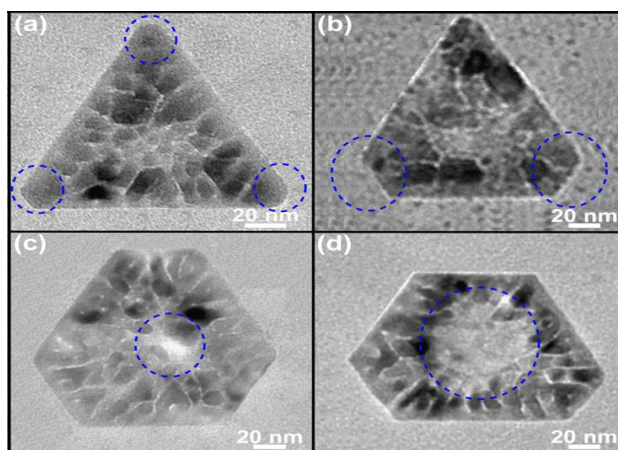

Fig. 6 Fig. 1. Shape evolution of 2-D ZnO nanopellets annealed for 90 minutes ((a) and (b)) and 120 minutes ((c) and (d)). (a) The highlighted circles indicate the truncated edges for a triangle nanopellet. (b) Diamond shape nanopellet with two truncated edges. (c) and (d) show the formation of a hole at the center of hexagonal nanopellets to form "ring structure" due to the etching effects of oleic acid

These improved truncated edges could be attributed to the surface energy reduction of the crystalline lattices due to the reason that the sharpening corner is highly unstable and requiring large amount of energy to retain its form [46]. From the perspective of advance technological applications, these truncated edges are believed to greatly and beneficially affect the absorption and scattering of light, which subsequently offer a new route for producing two-dimensional ZnO nanostructures with optimize plasmon resonance properties that is highly potential to be applied in molecular detection and

spectroscopy [47].

B. X-ray Diffraction (XRD)

The XRD pattern of the Fe_3O_4 nanocrystals is shown in Fig. 7. All the peaks are matched with standard sample (JCPDF: 72-2303). The nanocrystals exist in face-centre-cubic phases (with space group *Fd*-3*m*) internal structure. No peaks from impurities are observed and the spectrum shows the characteristics of finite size broadening effect in all reflections.
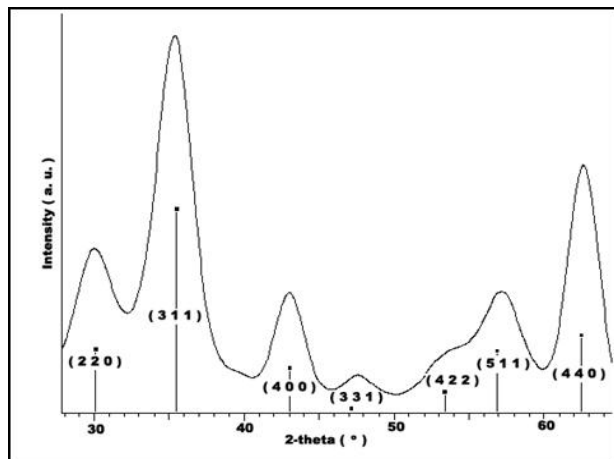

Fig. 7 XRD pattern of Fe_3O_4 nanocrystals (▪ is the standard diffraction peak)

The XRD pattern of ZnO annealed for 60 minutes and 90 minutes was shown in Fig. 8. All the peaks can be indexed to that of the standard ZnO with hexagonal wurtzite crystal structures (with space group *P63mc*) [48]. Meanwhile, no diffraction peaks from other impurities have been observed.This implies that all the $Zn(C_{18}H_{33}O_2)_2$ are fully decomposed into ZnO. Both samples shown in Fig. 8 merely consist of wurtzite crystal structures without any presence of zinc blende structures. This is because wurzite structure configuration has the Madelung constant 0.2 %, which is larger than that of zinc blende. Thus, the strong ionic compound likes ZnO favors for wurzite structures unless high pressure is applied [49-51].We have performed the d-spacing calculations by choosing the most dominant peak (hkl plane = 101) to determine the purities of the samples. Based on Bragg's equation ($d_{101} = n\lambda / 2 \sin \theta$), the calculated d-spacing, d_{101} for the samples annealed for 60 minutes and 90 minutes is 2.49 Å and 2.47 Å respectively. These values are comparable with that of the standard hexagonal phase crystalline structure, as can be calculated from equation 1[52]:

$$d'_{101} = \frac{a}{\sqrt{\frac{4}{3}(h^2 + hk + k^2) + l^2\left(\frac{a^2}{c^2}\right)}} \tag{1}$$

According to powder diffraction pattern, the reflective intensities from all the peaks are proportional to annealing duration. This implies that higher annealing treatment had improved the atomic ordering. Thermal energy activation that triggered the internal atomic diffusion to the correct position assists in developing a well-orientated crystal lattice [53].
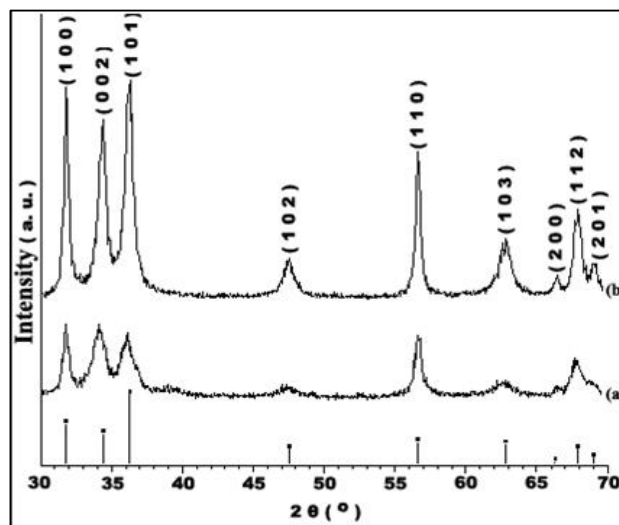

Fig. 8 XRD pattern of ZnO nanopellets annealed at (a) 60 minutes and (b) 90 minutes (▪ is the standard diffraction pattern)

These are well-correlated with TEM micrograph in Fig. 5 where majority of the nanopellets have well-defined shapes with flat edges if compared to the sample that was annealed for 60 minutes (Fig. 4). No phase transitions occur, even though after persistent annealing for 120 minutes was carried out except the increase in the intensity for each peak. In addition, no agglomerations or phase disruptions were observed for the samples although the drying and dispersing process were repeated for 3 times. Explicitly, both of these observations indicate that the nanopellets are more physically and chemically stable if compared to that being reported in the literature [35].

IV. CONCLUSION

Magnetic (Fe_3O_4) nanocrystals and semiconductor (ZnO) nanopellets have been successfully prepared by using palm-oil based compound (oleic acid) in non-hydrolytic phase via control thermal pyrolysis of organometalic compound. The current synthetic approach produces nanostructures with well-defined shapes. Furthermore, this method offers a safe and simple route for the synthesis of 2-dimensional nanopellets with high yield. Further development and extension of current synthetic strategy are being pursued to combine both of these materials into nanocomposite form that will be use as "smart magnetic nanophotocatalyst" for industry waste water treatment.

REFERENCES

[1] Wang, J., Gudiksen, M.S., Duan, X., Cui, Y., Lieber, C.M., (2001) "Highly polarized photoluminescence and photodetection from single indium phosphide nanowires", Science, 293, 1455–1457.

[2] Zhong, Z., Qian, F., Wang, D., Lieber, C.M., (2003) "Synthesis of p-type gallium nitride nanowires for electronic and photonic nanodevices", Nanoletters, 3 (3), 343–346.

[3] Hahm, J., Lieber, C.M., (2004) "Direct ultrasensitive electrical detection of DNA and DNA sequence variations using nanowire nanosensors", Nanoletters, 4 (1), 51–54.

[4] Alivisatos, A.P., (1996) "Semiconductor clusters, nanocrystals, and quantum dots", Science, 271, 933–937.

[5] Burda, C., Chen, X., Narayanan, R., El-Sayed, M.A., (2005) "Chemistry and properties of nanocrystals of different shapes", Chem. Rev., 105, 1025–1102.

[6] Zhitenev, N.B., Fulton, T.A., Yacob, A., Hess, H.F., Pfeiffer, L.N., West, K.W., (2000) "Imaging of localized electronic states in the quantum Hall regime", Nature, 404, 473–476.

[7] Suen, Y.W., Engel, L.W., Santos, M.B., Shayegan, M., Tsui D.C., (1992) "Observation of a ˆⅠ½ = 1/2 fractional quantum Hall state in a double-layer electron system", Phys. Rev. Lett., 68, 1379–1382.

[8] Stormer, H.L., (1998) "Fractional quantum Hall effect today", Solid State Commun., 107, 617–620.

[9] Stormer, H.L., Du, R.R., Kang, W., Tsui, D.C., Peeiffer, L.N., Baldwin, K.W., West, K.W., (1994) "The fractional quantum Hall effect in a new light", Semicond. Sci. Technol., 9, 1853–1858.

[10] Wang, Z.L., (2004) "Nanostructures of zinc oxide", Mater. Today, 7 (6), 26–33.

[11] Cao, H., Xu, J.Y., Zhang, D.Z., Chang, S.H., Ho, S.T., Seelig, E.W., Liu, X., Chang, R.P.H., (2000) "Spatial confinement of laser light in active random media", Phys. Rev. Lett., 84, 5584–5587.

[12] Bagnall, D.M., Chen, Y.F., Zhu, Z., Yao, T., Koyama, S., Shen, M.Y., Goto, T., (1997) "Optically pumped lasing of ZnO at room temperature", Appl. Phys. Lett., 70, 2032–2230.

[13] Yu, P., Tang, Z.K., Wong, K.L., Kawasaki, M., Ohtomo, A., Koinuma, H., Segawa, Y., (1998) "Room-temperature gain spectra and lasing in microcrystalline ZnO thin films", J. Cryst. Growth, 184/185, 601–604.

[14] Kayamura, Y., (1988) "Quantum-size effects of interacting electrons and holes in semiconductor microcrystals with spherical shape", Phys. Rev. B, 38, 9797–9805.

[15] Wegscheider, W., Pfeiffer, L.N., Dignam, M.M., Pinczuk, A. W., West, K., McCall, S.L., Hull, R., (1993) "Lasing from excitons in quantum wires", Phys. Rev. Lett., 71, 4071–4074.

[16] Garcia, M.A., Merino, J.M., Pinel, E.F., Quesada, A., Venta, J., Gonzalez, M.L.R., Castro, G.R., Crespo, P., Llopis, J., G-Calbet, J.M., Hernando, A., (2007) "Magnetic properties of ZnO nanoparticles", Nanoletters, 7, 1489–1494.

[17] Huang, M.H., Mao, S., Feick, H., Yan, H., Wu, Y., Kind, H., Weber, E., Russo, R., Yang, P., (2001) "Room-temperature ultraviolet nanowire nanolasers", Science, 292, 1879–1897.

[18] Wang, X., Song, J., Liu, J., Wang, Z.L., (2007) "Direct-current nanogenerator driven by ultrasonic waves", Science, 316, 102–105.

[19] Yang, P., (2005) "The chemistry and physics of semiconductor nanowires", Mater. Res. Bull., 30, 85–91.

[20] Greene, L.E., Law, M., Tan, D.H., Montano, M., Goldberger, J., Somorjai, G., Yang P., (2005) "General route to vertical ZnO nanowire arrays using textured ZnO seeds", Nanoletters, 5 (7), 1231–1236.

[21] Shen, G., Cho, J.H., Yoo, J.K., Yi, G.C., Lee, C.J., (2005) "Synthesis and optical properties of S-doped ZnO nanostructures: nanonails and nanowires", J. Phys. Chem. B, 109, 5491–5496.

[22] Garti, N., Aserin, A., Tiunova, I., Fanun, M., (2000) "A DSC study ofwater behavior inwaterin-oil microemulsions stabilized by sucrose esters and butanol", Colloid Surf. A, 170, 1–18.

[23] Khiew, P.S., Huang, N.M., Radiman, S., Ahmad, M.S., (2004) "Synthesis of NiS nanoparticles using a sugar–ester nonionicwater-in-oil microemulsion", Mater. Lett., 58, 516–521.

[24] Khiew, P.S., Radiman, S., Huang, N.M., Ahmad, M.S., (2005) "Preparation and characterization of ZnS nanoparticles synthesized from chitosan laurate micellar solution", Mater. Lett., 59, 989–993.

[25] Huang, N.M., Radiman, S., Khiew, P.S., Laggner, P., Kan, C.S., (2004) "In situ templating of PbS nanorods in reverse hexagonal liquid crystal", Colloids Surf. A, 247, 55–60.

[26] Khiew, P.S., Radiman, S., Huang, N.M., Ahmad, M.S., (2004) "Synthesis and characterization of copper sulfide nanoparticles in hexagonal phase lyotropic liquid crystal", J. Cryst. Growth, 268, 227–237.

[27] Khiew, P.S., Radiman, S., Huang, N.M., Ahmad, M.S., (2003) "Studies on the growth and characterization of CdS and PbS nanoparticles using sugar–ester nonionic water-in-oil microemulsion", J. Cryst. Growth, 254, 235–243.

[28] Khiew, P.S., Radiman, S., Huang, N.M., Ahmad, M.S., (2004) "In situ polymerization of conducting polyaniline in bicontinuous cubic phase of lyotropic liquid crystal", Colloids Surf. A-Physicochem. Eng. Asp., 247, 35–40.

[29] Huang, N.M., Kan, C.S., Khiew, P.S., Radiman, S., (2004) "Single w/o microemulsion templating of CdS nanoparticles", J. Mater. Sci., 39, 2411–2415.

[30] Khiew, P.S., Huang, N.M., Radiman, S., Ahmad, M.S., (2004) "Synthesis of NiS nanoparticles using a sugar–ester nonionicwater-in-oil microemulsion", Mater. Lett., 58 , 762–767.

[31] Chiu, W. S., Khiew, P. S., Isa, D., Cloke, M., Radiman, S., Abd-Shukor, R., Abdullah, M. H., Huang, N. M. (2008) "Synthesis of two-dimensional ZnO nanopellets by pyrolysis of zinc oleate" Chem. Eng. J., 142(3), 337-343.

[32] Hirano, S., Masuya, K., Kuwabara, M., (2004) "Multi-nucleation-based formation of oriented zinc oxide microcrystals and films in aqueous solutions", J. Phys. Chem. B, 108, 4576–4578.

[33] Kuo, C.L., Kuo, T.J., Huang, M.H., (2005) "Hydrothermal synthesis of ZnO microspheres and hexagonal microrods with sheetlike and platelike nanostructures", J. Phys. Chem. B, 109 (43), 20115–20121.

[34] Yoshida, T., Tochimoto, M., Schlettwein, D., Wohrle, D., Sugiura, T., Minoura, H., (1999) "Self-assembly of zinc oxide thin films modified with tetrasulfonated metallophthalocyanines by one-step electrodeposition", Chem. Mater., 11, 2657–2667.

[35] Pinna, N., Weiss, K., Kongehl, H.S., Vogel, W., Urban, J., Pileni, M.P., (2001) "Triangular CdS nanocrystals: synthesis, characterization, and stability", Langmuir, 17, 7982–7987.

[36] Fons, P., Tampo, H., Kolobov, A.V., Ohkubo, M., Niki, S., Tominaga, J., Carboni, R., Boscherini, F., Friedrich, S., (2006) "Direct observation of nitrogen location in molecular beam epitaxy grown nitrogen-doped ZnO", Phys. Rev. Lett., 96, 045504–045505.

[37] Chiu, W.S., Radiman, S., Abdullah, M.H., Khiew, P.S., Huang, N.M., Abd-Shukor, R., (2007) "One pot synthesis of monodisperse Fe3O4 nanocrystals by pyrolysis reaction of organometallic compound", Mater. Chem. Phys., 106, 231–235.

[38] Peng, X., (2003) "Mechanisms for the shape-control and shape-evolution of colloidal semiconductor nanocrystals", Adv. Mater., 15 (5), 459–463.

[39] Yu, W.W., Wang, Y.A., Peng, X., (2003) "Formation and stability of size-, shape-, and structure-controlled CdTe nanocrystals: ligand effects on monomers and nanocrystals", Chem. Mater., 15, 4300–4308.

[40] Yu, W.W., Peng, X., (2002) "Formation of high-quality CdS and other II–VI semiconductor nanocrystals in noncoordinating solvents: tunable reactivity of monomers", Angew. Chem. Int. Ed., 41 (13), 2368–2371.

[41] Wang, Z.L., Kong, X.Y., Zuo, J.M., (2003) "Induced growth of asymmetric nanocantilever arrays on polar surfaces', Phys. Rev. Lett., 91 (18), 185502–185505.

[42] Chiu, W.S., Radiman, S., Abd-Shukor, R., Abdullah, M.H., Khiew, P.S., (2008) "Tunable coercivity of CoFe2O4 nanoparticles via thermal annealing treatment", J. Alloy Comp., 459, 291–297.

[43] Bovin, J.O., Wallember, R.L., Smith, D., (1985) "Imaging of atomic clouds outside the surfaces of gold crystals by electron microscopy", Nature, 317, 47–49.

[44] Iijima, S., Ichihashi, H., (1986) "Structural instability of ultrafine particles of metals", Phys. Rev. Lett., 56, 616–619.

[45] Zhu, H., Averback R.S., (1996) "Sintering processes of two nanoparticles: a study by molecular dynamics simulations", Philos. Magn. Lett., 73, 27–33.

[46] Wiley, B.J., Im, S.H., Li, Z.Y., McLellan, J., Siekkinen, A., Xia, Y., (2006) "Maneuvering the surface plasmon resonance of silver nanostructures through shape-controlled synthesis", J. Phys. Chem. B, 110, 15666–15675.

[47] Kelly, K.L., Corondo, E., Zhao, L.L., Sxhatz, G.C., (2003) "The optical properties of metal nanoparticles: the influence of size, shape, and dielectric environment", J. Phys. Chem. B, 107, 668–677.

[48] Joint Committee for Powder Diffraction Society (JCPDS), Powder Diffraction Database, pattern: 36-1451.

[49] Yeh, C.Y., Lu, Z.W., Froyen, S., Zunger, A., (1992) "Zinc-blende? wurtzite polytypism in semiconductors", Phys. Rev. B, 46, 10086–10097.
[50] Yeh, C.Y., Wei, S.H., Zunger, A., (1994) "Relationships between the band gaps of the zincblende and wurtzite modifications of semiconductors", Phys. Rev. B, 50, 2715–2718.
[51] Serrano, J., Romero, A.H., Manjon, F.J. ´, Lauck, R., Cardona, M., Rubio, A., (2004) "Pressure dependence of the lattice dynamics of ZnO: an ab initio approach", Phys. Rev. B, 69, 094306–094319.
[52] Shackelford, J.F., Introduction toMaterial Science for Engineers, 6th ed., Pearson-Prentice Hall, USA, 2004, p. 106.
[53] Yeh, C.Y., Wei, S.H., Zunger, A., (1994) "Relationships between the band gaps of the zincblende and wurtzite modifications of semiconductors", Phys. Rev. B, 50, 2715–2718.